

**AN EDITED VERSION OF THIS PAPER WAS PUBLISHED BY AGU.
COPYRIGHT (YEAR) AMERICAN GEOPHYSICAL UNION.**

**FURTHER REPRODUCTION OR ELECTRONIC DISTRIBUTION IS NOT
PERMITTED**

**A soil-water retention function that includes the hyper-dry region
through the BET adsorption isotherm**

Orlando Silva¹ and Jordi Grifoll^{*}

Grup de recerca de Fenòmens de Transport
Departament d'Enginyeria Química,
Universitat Rovira i Virgili,
Av. dels Països Catalans 26,
43007 Tarragona, Spain.

^{*}Corresponding author. Tel.: +34 977 55 96 39; fax +34 977 55 96 21
E-mail addresses:

osilva@ija.csic.es (O. Silva), jordi.grifoll@urv.cat (J. Grifoll)

¹ Present address: Institut de Ciències de la Terra Jaume Almera (CSIC),
Lluís Solé i Sabarís s/n, 08028 Barcelona, Spain

1 **Abstract**

2 Most existing full-range soil-water retention functions extend standard capillary
3 pressure curves into the dry region to zero water content at a finite matric pressure. A
4 description of dryness is commonly taken as oven-dry conditions given by a matric suction of
5 about 10^9 Pa at zero liquid saturation. However, no finite pressure can be exerted by a zero
6 amount of water, so a possibly more realistic situation necessarily implies that as water
7 content approaches zero, suction tends to infinity. In this study we propose a full-range water
8 retention function that takes advantage of the physical consistence of the Brunauer-Emmett-
9 Teller (BET) adsorption isotherm to describe the very dry end, and preserves the capillary
10 behavior of the classical Brooks and Corey function in the wet range. The transition from
11 capillary to adsorption mechanisms is accounted for by a generalization of the Bradley's
12 isotherm. Tests on seven widely studied soil data sets show that the experimental water
13 retention curves are well fitted by the proposed retention model. In order to test the present
14 approach, our simulations were compared to experimental data, for water transport under dry
15 conditions, found in the literature. The present model was also compared with a recently
16 proposed extended retention function in a hypothetical experiment designed to test the
17 influence of predicted soil humidity on solute volatilization. These comparisons showed that,
18 under severe dryness, the water dynamics is well described by the proposed model. Moreover,
19 in these conditions the retention function determines the soil humidity, to which solute
20 volatilization calculations can be very sensitive.

21 **1. Introduction**

22 Simulation of water flow and chemical transport in the vadose zone requires soil-water
23 retention (SWR) models. These are mathematical descriptions of the relationship between
24 matric suction and water content. The two most frequently used SWR models have been those
25 proposed by *Brooks and Corey* [1964] (BC) and *van Genuchten* [1980] (VG). Their
26 popularity is due to their ability to fit water retention experimental data in the wet region,
27 where it is often expected that most flow occurs, and owing to the fact that they can also be
28 readily combined with conductivity models [e.g., *Burdine*, 1953; *Mualem*, 1976] in order to
29 yield analytic expressions for relative permeability.

30 Application of BC and VG functions is generally unsuitable for the very dry range
31 (matric pressure < -1.5 MPa) [*Nimmo*, 1991; *Ross et al.*, 1991]. In fact, one of the
32 disadvantages of the traditional water retention models is that they do not allow water content
33 to be below the "residual water content parameter", an assumption that is physically
34 unrealistic [*Nimmo*, 1991; *Groenevelt and Grant*, 2004]. This may imply little or no difficulty
35 for some applications, such as wetland studies or humid region agriculture, but others,
36 including water flow and solute transport in arid and semi-arid regions, require a more
37 realistic representation of the hydraulic characteristics over the whole range of saturation. For
38 the fine-textured media the high-suction range can be relevant even when water content
39 remains high.

40 Empirical extensions for the dry range have been given by several authors. *Ross et al.*
41 [1991] modified the *Campbell* [1974] SWR model to extend the retention curve to dryness.
42 They compared their model with the original equation of Campbell, which was extrapolated
43 to oven-dry conditions, finding that the new function fitted experimental data better than the
44 original equation. *Campbell et al.* [1993] showed that their simple linear relationship for the
45 water sorption isotherm [*Campbell and Shiozawa*, 1992] fits experimental data as well as the

46 more complex model of *Fink and Jackson* [1973]. *Rossi and Nimmo* [1994] (RN) presented a
47 sum and a junction model, both based on a power law function complemented with a
48 logarithmic function in the dry range. The sum model adds these two components, while the
49 junction model matches them. In both models the continuity of the function and its derivative
50 is assured. Good agreement between both models and seven sets of experimental water
51 retention data was obtained. *Fayer and Simmons* [1995] proposed replacing the residual water
52 content in the BC and van Genuchten functions with the simple water adsorption equation
53 given by *Campbell and Shiozawa* [1992]. *Morel-Seytoux and Nimmo* [1999] (MS-N)
54 extended the BC model into the high suction range using the *Rossi and Nimmo* [1994]
55 junction model. *Webb* [2000] presented a method to extend classical retention functions to
56 zero liquid saturation, without the need to refit the experimental data as in other approaches
57 [*Rossi and Nimmo*, 1994]. *Groenevelt and Grant* [2004] proposed a model that covers the
58 complete retention curve, expressed in terms of the pF scale previously introduced by
59 *Schofield* [1935]. These authors fitted their model to a variety of soils, finding good
60 agreement between experimental data and their SWR function over the whole range of
61 saturation. As *Rossi and Nimmo* [1994] have pointed out, one of the advantages in having a
62 full-range model of water retention is that it can reliably extrapolate the water retention curve
63 beyond the driest measured point, which can help save measurement time at high suctions.
64 However, although these new whole range approaches give a more accurate representation in
65 the dry end, they have the disadvantage of allowing water content to be zero at finite suction
66 [*Rossi and Nimmo*, 1994; *Morel-Seytoux and Nimmo*, 1999; *Groenevelt and Grant*, 2004]. For
67 laboratory conditions (e.g., oven drying at 105°-110 °C in a room at 50% relative humidity),
68 zero water content is defined as oven dryness, which corresponds to a finite suction, generally
69 taken as $\sim 10^3$ MPa. Although in most applications and from the practical point of view it is
70 difficult to perceive differences in the calculated soil behavior at very high, but finite, matric

71 suctions, the theory of the thermodynamic equilibrium states that as absolute dryness is
72 approached, the matric suction must tend to infinity [e.g. *Baggio et al.*, 1997].

73 In an effort to provide a full-range SWR function that overcomes these difficulties,
74 *Tuller et al.*, [1999] and *Or and Tuller*, [1999] proposed a pore space representation (angular
75 pore space model) that accommodates both capillarity and adsorptive processes on internal
76 surfaces. This alternative approach enables consideration of individual contributions of
77 capillary and adsorptive components to soil water matric pressure through the whole range of
78 saturation, and even satisfies the condition of zero water content at infinite suction. However,
79 its implementation in a numerical transport model is cumbersome and many parameters need
80 to be fitted for a particular soil.

81 While the new full-range functions provide improved representations of the SWR
82 characteristic, their use and evaluation in numerical transport models has been limited. So far
83 the study of *Andraski and Jacobson* [2000] seems to be the one that has explicitly tested the
84 performance of a full-range water-retention function. These authors altered the UNSAT-H
85 numerical model [*Fayer and Jones*, 1990] to incorporate the *Rossi and Nimmo* [1994] water-
86 retention function. Then they compared field measured and simulated water and heat transport
87 in a layered soil during a period of 3.85 years. Their results showed that simulations using the
88 RN approach compared favorably with those using the traditional BC model and that RN
89 function can improve the prediction of water potentials in near-surface soils, particularly
90 under dry conditions.

91 It is well known [*Chiou and Shoup*, 1985; *Chen et al.*, 2000a and 2000b; *Chen and*
92 *Rolston*, 2000] that chemical sorption on nearly dry soils (saturations lower than 0.1) is
93 greatly influenced by relative humidity. Therefore, it is expected that a physically accurate
94 description of the moisture behavior in a very dry soil could also help improve chemical and
95 water transport simulations. In particular, an appropriate description of the SWR under hyper-

96 dry conditions is important for water behavior to be accurately predicted at and near the soil
97 surface. Estimating evaporation and recharge rates can, therefore, be critical [e. g. *Scanlon et*
98 *al.*, 2003; *Agam and Berliner*, 2006]. Another area in which a SWR function extended to
99 dryness can be useful is the remediation of volatile organic compounds by soil vapor
100 extraction or venting strategies. When these techniques are used, water movement and
101 competitive sorption between hydrocarbon and water vapors take place simultaneously
102 [*Batterman et al.*, 1995]. The description of these phenomena may potentially be important
103 near the upper surface of the soil, in the vicinity of air injection wells, and in arid
104 environments [*Yoon et al.*, 2003]. This function can also play an important role in the area of
105 materials science, where porous materials need to function under very dry conditions [e.g.
106 *Gawin et al.*, 2002; *Schrefler*, 2004]. The available extended SWR functions are not always
107 able to describe the soil-water state in very dry conditions. For instance, *Goss and Madliger*
108 [2007] found that the Rossi-Nimmo retention function does not satisfactorily fit their
109 experimental data. For practical purposes, they fitted the data with a third-order polynomial,
110 although they recognized that the type of function they chose has no mechanistic meaning
111 [*Goss and Madliger*, 2007].

112 In this paper, a robust and physically meaningful full-range SWR function is proposed.
113 In addition of accommodating the BC functionality in the wet range of the curve, this
114 proposed function is in accordance with the Brunauer-Emmett-Teller (BET) adsorption
115 isotherm in the dry range. A smooth transition from pure adsorption to pure capillarity is
116 accomplished by a generalization of Bradley's isotherm. To assess the accuracy and
117 suitability of the present approach, we implemented the new water retention function in a
118 transport model, and checked its performance in a water transport, and water and chemical
119 transport numerical simulations.

120

121 **2. Soil-Water Retention Model**

122 We constructed our proposed SWR function for the whole range of suctions by linking
123 three individual functions for specific suction ranges, much like the two-parameter junction
124 model approach of *Rossi and Nimmo* [1994]. Three ranges are differentiated through the
125 transition matric pressures, P_1 and P_2 (Pa), which define the transition between capillary-
126 adsorptive and adsorptive-hyperadsorptive behavior. The individual functions are the Brooks-
127 Corey function, (from saturation to P_1), a generalization of Bradley's adsorption isotherm
128 (from P_1 to P_2), and the BET adsorption isotherm (from P_2 to infinite suction). Note that in
129 the wet region, the relationship between the matric pressure P (Pa) and the volumetric water
130 content θ_w can be taken from any retention function that has proved to be acceptable in the
131 region. In this study we have considered the original BC model for simplicity. Unlike *Rossi*
132 *and Nimmo* [1994] who adopted a parabolic correction near saturation, we considered the
133 conventional BC including the air-entry pressure at saturation. This parabolic correction, or
134 more elaborate proposals such as MS-N, can be used if a detailed description near saturation
135 is needed.

136 Whereas in the wet range the SWR curve is the expression of capillary forces, in the
137 dry range, adsorption dominates the relationship between water content and the forces that
138 hold this water in its condensed state. Water adsorption onto soils has been studied by
139 different authors [*Puri et al.*, 1925; *Orchiston*, 1952; *Chiou and Shoup*, 1985; *Valsaraj and*
140 *Thibodeaux*, 1988; *Rhue et al.*, 1989; *Pennell et al.*, 1992; *Amali et al.*, 1994; *Ruiz et al.*,
141 1998; *Chen et al.*, 2000; *de Seze et al.*, 2000] and it has been shown that it can be described by
142 the conventional BET isotherm [*Valsaraj*, 1995]. This adsorption isotherm is written here as

$$144 \frac{\theta_w}{\theta_{wm}} = \frac{Bx}{(1-x)[1+(B-1)x]} \quad (1)$$

145

146 where

$$147 \quad \theta_{wm} = W_m (1 - \varepsilon) \rho_s / \rho_w \quad (2)$$

148

149 is a pseudo-volumetric water content at monolayer capacity. Also in (2), ρ_s (kg/m³) is the
150 density of the solid-soil phase, ρ_w (kg/m³) is the density of the water, and ε (m³/m³) is the
151 porosity. The mass monolayer capacity W_m (kg/kg) and B are characteristic BET isotherm
152 parameters and x is the relative humidity of the air-soil. W_m , the surface index, is the mass of
153 water required to cover the surface completely as a monolayer, while B is the index of the
154 average net heat of adsorption in the first layer [Orchiston, 1952]. In the absence of osmotic
155 pressure effects, the relative humidity is related to the matric pressure according Kelvin's
156 equation [e.g. Bear and Batchmat, 1991]

157

$$158 \quad x = \exp\left(\frac{P \hat{V}_w}{R T}\right) \quad (3)$$

159

160 where \hat{V}_w (m³/mol) is the liquid molar volume of water, R is the universal gas constant (Pa
161 m³/K mol) and T (K) is the temperature. If osmotic pressure effects are present, equation (3)
162 can be modified to include them. This can be done, for instance, using the more general
163 thermodynamic-based relationship given by Burns *et al.* [2000a, 2000b], which describes the
164 influence of free dissolved salts on water vapor pressure and liquid pressure in unsaturated
165 soils.

166 The matric pressure definition can be extended to include adsorption considering

167

168
$$P = -\frac{\Delta h}{\hat{V}_w} \quad (4)$$

169

170 as *Baggio et al.* [1997] suggested, where Δh (J/mol) is the enthalpy difference between water
 171 vapor in the gas-phase and the condensed or adsorbed liquid-phase, excluding the latent
 172 enthalpy of vaporization. Adopting this definition, matric pressure and Kelvin's equation can
 173 be applied in SWR curves in the range of low water contents [*Gawin et al.*, 2002; *Schrefler*,
 174 2004]. Note that in the present model the water content is counted from absolute dryness,
 175 although most experimental data in the literature are based on the water content set at zero at a
 176 matric suction of $\sim 10^3$ MPa, where some water molecules are still present in the soil.

177 Our proposal is to use equations (1) and (3) as the part of the SWR curve applicable in
 178 the "dry" region. Using this approach, water adsorption onto soils and soil-water characteristic
 179 curves at low moisture content will be described by the same mechanism and formulation.

180 Altogether, there are three different regions to be considered throughout the range of
 181 the retention curve: (i) a reliable function at high water content where the capillary
 182 mechanism is dominant. For purposes of simplicity, in this study we have used the power law
 183 relationship proposed by *Brooks and Corey* [1964],

184

185
$$\theta_w = \varepsilon, \quad P \geq P_b \quad (5a)$$

186
$$\frac{\theta_w - \theta_r}{\varepsilon - \theta_r} = \left(\frac{P}{P_b} \right)^{-\lambda}; \quad P_1 \leq P \leq P_b \quad (5b)$$

187

188 (ii) a logarithmic behavior at low and medium water contents where multilayer adsorption
 189 progressively dominates capillary forces

190

191
$$\ln(-P) = a + b\theta_w + c\theta_w^2 + d\theta_w^3; P_2 \leq P \leq P_1 \quad (6)$$

192

193 and (iii) a final adsorption region described by the BET isotherm as given in equations (1)-(3)
 194 for $P < P_2$.

195 When c and d are zero, equation (6) reduces to the Bradley's adsorption isotherm
 196 [Bradley, 1936], which has been demonstrated to be in good agreement with experimental
 197 data [e.g. *Orchiston*, 1952]. Indeed, the extension of this equation to dryness was the basic
 198 assumption used by *Rossi and Nimmo* [1994] to develop their model.

199 To apply the present model for a given soil, the BET isotherm parameters (W_m , B) and
 200 the Brooks and Corey parameters (P_b , θ_r , λ , ε) must be known or fitted. This is an acceptable
 201 number of parameters considering that two different phenomena are described by the same
 202 curve. Available experimental data of water adsorption on various soils [e.g., *Orchiston*,
 203 1952; *Amali et al.* 1994; *de Seze et al.*, 2000] shows that BET equation (1) gives a good
 204 representation up to $x = 0.3$. This is a reasonable value which is based on the study by *de Seze*
 205 *et al.* [2000], who note that for $x > 0.5$ the BET isotherm over-predicts the experimental data.
 206 On the other hand, most hydraulic retention models, including BC and VG, fit the
 207 experimental data reasonably well at least up to the "permanent wilting point". Generally, the
 208 permanent wilting point is assumed to be at a suction of 1.5 MPa, although in reality plant
 209 water stress depends on plant, soil and atmospheric conditions [*Cassel and Nielsen*, 1986].
 210 Therefore, as a general rule, we have assumed that equation (6) for intermediate behavior is
 211 valid between the junction matric pressure $P_2 \approx -162$ MPa (at 20 °C), corresponding to a
 212 relative humidity of $x_2 = 0.3$, and the junction matric pressure $P_1 = -1.5$ MPa. Thus, the
 213 remaining unknown parameters (a , b , c , d) can be calculated from the conditions that ensure
 214 continuity of θ_w and its first derivative at P_1 between (5) and (6), and at P_2 between (6) and

215 (1). Designating by θ_{w1} and θ_{w2} the volumetric water content at each matching point, these
 216 continuity equations are expressed as

217

$$218 \quad a + \theta_{w1}b + \theta_{w1}^2c + \theta_{w1}^3d = \ln(-P_1) \quad (7a)$$

$$219 \quad b + 2\theta_{w1}c + 3\theta_{w1}^2d = -\frac{1}{\lambda(\theta_{w1} - \theta_r)} \quad (7b)$$

$$220 \quad a + \theta_{w2}b + \theta_{w2}^2c + \theta_{w2}^3d = \ln(-P_2) \quad (7c)$$

$$221 \quad b + 2\theta_{w2}c + 3\theta_{w2}^2d = \frac{(1-x_2)^2[1+(B-1)x_2]^2}{\theta_{wm}Bx_2 \ln(x_2)[1+(B-1)x_2^2]} \quad (7d)$$

222

223 Of course, the junction matric pressures P_1 and P_2 may be taken as fitting parameters.
 224 However, we have preferred to fix them, because this keeps the model simple and because the
 225 experimental data available supports these values.

226 A list of experimental water adsorption BET parameters in soils taken from the
 227 literature is given in Table 1. It is apparent that these parameters are soil dependent, with a
 228 range of values given by $0.04 \text{ mg/g} \leq W_m \leq 39.8 \text{ mg/g}$ and $5 \leq B \leq 128.07$. In the absence of
 229 experimental data, one could take as a first estimate the average of the values listed in
 230 Table 1, which are $W_m = 13.4 \text{ mg/g}$ and $B = 23.8$. The parameters λ , θ_r , ε and P_b of the BC
 231 retention curve are also soil dependent. Fortunately, there are procedures for estimating these
 232 parameters from other, more easily measurable, soil properties. For instance, *Rawls and*
 233 *Brakensiek* [1989] gave the average BC parameter values for the different soil textural classes
 234 in addition to correlations for estimating these BC parameters from porosity and the clay and
 235 sand percentages.

236 However, when experimental data is available, the normal procedure we propose
237 consists of two steps. First, one has to fit the BET adsorption isotherm (parameters W_m, B) in
238 the range of relative humidity below $x_2 = 0.30$ through the common procedure described by
239 other authors [e.g. *Chen et al.*, 2000a; *de Seze et al.*, 2000]. The second step is to fit the set of
240 parameters ($\lambda, \theta_r, \varepsilon, P_b$) minimizing the global error of the piecewise SWR function, with the
241 set of parameters (a, b, c, d) determined by solving the linear system of equations (7). In the
242 majority of cases, porosity is a measured parameter, which reduces to three the number of BC
243 parameters to be fitted. The present piecewise water retention curve was fitted to six data sets
244 from *Campell and Shiozawa* [1992] and one data set from *Schofield* [1935]. The same data
245 sets were used by *Rossi and Nimmo* [1994] and *Morel-Seytoux and Nimmo* [1999] to check
246 their models. Figure 1 shows good agreement between the present SWR curve and the
247 corresponding soil experimental data set. In this figure, the horizontal dashed lines define the
248 locations of matching points at P_1 and P_2 . To fit the BC parameters logarithmic
249 transformation was used to provide variance homogeneity. The objective function of the
250 optimization was the square of the root mean square error (RMSE)

251

$$252 \quad \text{RMSE} = \sqrt{\frac{1}{N} \sum_{i=1}^N [\log(-M_i) - \log(-P_i)]^2} \quad (8)$$

253

254 where M_i and P_i are measured and predicted values of the matric pressure, respectively, and N
255 is the total number of measurements. The Generalized Reduced Gradient algorithm [*Lasdon et*
256 *al.*, 1978] was used to minimize the objective function, equation (8). The fitting parameters
257 for each soil obtained by the strategy described above are given in Table 2. Additionally, we
258 have included in Table 3 the R^2 values for the BET fit, the RMSE (Eq. 8), and the maximum
259 and average θ_w discrepancies between the present approach and the experimental data,

260 calculated in the range of matric pressure lower than -1.5 MPa. For comparison, the MS-N
261 model fits were also included in Figure 1. Below P_1 , both models apparently fit the
262 experimental data equally well. Close to saturation, the MS-N model uses a third order
263 polynomial. Then it is not surprising that for some soils, as the L -Soil (Figure 1f), MS-N fits
264 the experimental data better than BC. A major difference between the present model and other
265 approaches is the behavior of the curve as θ_w tends to zero. Whereas most of the other full-
266 range functions have the limiting suction value of $\sim 10^3$ MPa (taken as oven dryness), the
267 present proposal tends to infinite suction in accordance with adsorption theories. It should be
268 noted that this limiting suction value of 10^3 MPa, taken for *Morel-Seytoux and Nimmo* [1999],
269 can not be regarded as universal, contrary to what *Groenevelt and Grant* [2004] state. For
270 instance, for soil #7 (Rothamsted) of the data set used by *Morel-Seytoux and Nimmo* [1999]
271 they had to change the limiting suction value to 5×10^3 MPa to conveniently fit the retention
272 curve, and *Chen et al.* [2000] fitted a Bradley's isotherm to their experimental data of
273 adsorption of water on Yolo silt loam soil, at 24.5 °C, obtaining a limiting suction of 1.7×10^3
274 MPa. For most practical purposes the logarithmic law, expressed in the form of the Bradley's
275 isotherm, represents the state of the soil system in the dry end very well. However, it has the
276 inconvenience of predicting a non-physical situation of finite matric pressure at zero water
277 content. It should be borne in mind that this is a "fictitious" zero water content, since it has
278 been defined as the water content present while the relative humidity in the soil is 1%,
279 achieved by setting a given combination of temperature and relative humidity in the
280 laboratory [*Schofield, 1935; Groenevelt and Grant, 2004*]. One of the advantages of the
281 present approach is that it overcomes this inconsistency, because in the very dry range the
282 BET adsorption isotherm governs the relationship between matric pressure and water content.
283 Another advantage of the present approach is that it captures the correct water retention
284 behavior in very dry conditions, as shown in Figure 2. In this figure, saturation, defined as

285 $S = \theta_w / \varepsilon$, is presented versus x , in the range of relative humidities lower than 100%, for L-
286 Soil and Royal soils (see Figure 1e-f). For comparison, the present approach, the MS-N model
287 and the experimental data are included. The representation of the water retention curve on the
288 BET scale shows that, for these soils, the MS-N retention model significantly underestimates
289 water saturation while the present approach fits the experimental data well.

290 Note that for all soils in Figure 1 the proposed SWR shows an abrupt change in the
291 present retention function near 10^3 MPa ($x = 0.0007$), coinciding with the experimental oven-
292 dryness suction. It should be noted that below this x value, the BET isotherm can be well
293 approximated by the straight line $\theta_w = B\theta_{wm}x$. This behavior is very similar to the behavior
294 shown by the modification to the Rossi-Nimmo two-parameter junction model proposed by
295 *Grant and Sletten* [2002]. These authors stated that for the soils studied by *Campbell and*
296 *Shiozawa* [1992], the relationship proposed by *Rossi and Nimmo* [1994] for the dry end
297 differs from the actual behavior of these soils, for which water content was an exponential
298 function of capillary pressure. Accordingly, *Grant and Sletten* [2002] suggested a
299 modification based on the relation between water vapor pressure and the nominal adsorbed
300 water thickness. It is interesting to note that they recognized a shortcoming in this relation: it
301 calculates a minute, but nonzero, water content at infinite capillary pressure.

302

303 **3. Testing the soil-water retention function in transport models**

304 In order to test the accuracy of present approach, we have incorporated the new SWR
305 function in a water and chemical transport numerical simulator. A suitable simulation scenario
306 must involve very low water content conditions, for which BET adsorption mechanism
307 governs the relationship between matric pressure and moisture. The testing exercise is divided
308 into two parts. In section 3.1, we first present the governing equations used in the water

309 transport model and details of the numerical implementation. Then, we use this model and our
310 SWR function to simulate one of the experiments of *Chen et al.* [2000b] for initial low water
311 content. This experiment involved the continuous evaporation of a soil column under
312 atmospheric conditions of varying relative humidity. Therefore, at least close to the soil
313 surface where evaporation occurs, the soil was expected to reach conditions of very low liquid
314 content ($S < 0.10$), for which SWR will be dominated by the BET branch of the present
315 approach (Eq. (1)). Finally, in section 3.2, we present the solute transport governing equations
316 and then the simulation of a hypothetical experiment of water evaporation leading to very dry
317 conditions in the soil, followed by the volatilization of an ethanol-contaminated layer. The
318 behavior of the present model is compared to the MS-N retention function in order to
319 demonstrate that under severe dryness conditions the present approach can also help improve
320 chemical transport and volatilization simulations.

321

322 **3.1. Water transport simulation**

323

324 **3.1.1. Governing equations and numerical implementation**

325 The unsaturated soil system considered consists of liquid (l), gas (g) and solid (s)
326 phases. When deriving the transport model equations, we assume that (i) the soil system is
327 under isothermal conditions, (ii) the water is in equilibrium in all phases at all times, (iii) the
328 advection in the gas-phase is negligible and (iv) spatial variations are only considered in z
329 direction (depth). The mass-conservation equation for water can be described by [*Silva and*
330 *Griffoll, 2007*]

331

$$332 \quad \frac{\partial}{\partial t} (\theta_w \rho_w + \theta_g \rho_v) = - \frac{\partial}{\partial z} (\rho_w q_l + J_{Wg}) \quad (9)$$

333

334 where ρ_w (kg/m³) is the liquid water density, θ_i (m³/m³) is the volumetric fraction of phase i
335 ($i = w, g$), ρ_v (kg/m³) is the water vapor density, and q_l (m/s) is the specific discharge of the
336 liquid-phase, which is given by the generalized Darcy's law [*Bear and Bachmat, 1991*]

337

$$338 \quad q_l = -\frac{k k_{rw}}{\mu_w} \left(\frac{\partial P}{\partial z} - \rho_w g \right) \quad (10)$$

339

340 In equation (10), k is the intrinsic permeability of the soil (m²), g (m/s²) is the gravity
341 acceleration, k_{rw} is the relative permeability (dimensionless) and μ_w (kg/m-s) is the dynamic
342 viscosity of water. The diffusive mass flux of water vapor, J_{wg} , is expressed as [*Bear and*
343 *Bachmat, 1991*]

344

$$345 \quad J_{wg} = -\theta_g D_{wg} \frac{\partial \rho_v}{\partial z} \quad (11)$$

346

347 where D_{wg} (m²/s) is the effective water vapor diffusion coefficient in the air within the porous
348 medium. The tortuosity was calculated using Millington and Quirk's first model as
349 recommended by *Jin and Jury* [1996]. The water vapor density was calculated assuming ideal
350 gas behavior and correcting for the curvature effect of the gas-liquid interface, as stated by
351 Kelvin's equation [*Bear and Bachmat, 1991*]

352 A dynamic boundary condition at the surface was set to accommodate the evaporation
353 flux, N_{w0} (kg/m² s). This flux was calculated by considering a mass transfer limitation from
354 the soil surface to the bulk atmosphere [*Brutsaert, 1975; Grifoll and Cohen, 1994*]

355

356
$$N_{w0} = k_{w0}(\rho_{wbk} - \rho_{v0}) \quad (12)$$

357

358 where k_{w0} (m/s) denotes the atmosphere-side mass transfer coefficients for water, ρ_{wbk}
359 (kg/m^3) is the background water vapor density in the atmosphere, while ρ_{v0} (kg/m^3) is the
360 water vapor density at the soil surface. The boundary condition at the bottom was set as zero
361 flux of water.

362 The governing partial differential equation for water transport (Eq. 9) was discretized
363 spatially and temporally in algebraic form using the finite volume method with a fully implicit
364 scheme (backward Euler) for time integration [Patankar, 1980]. The non-linear discretized
365 governing equation was solved for the matric pressure using the multivariable Newton-
366 Raphson iteration technique [Kelley, 1995], with a finite difference approximation of the
367 Jacobian coefficient matrix [Kelley, 1995; Press et al., 1986-1992] and the numerical
368 algorithm described by Silva and Grifoll [2007]. The total soil depth of the simulation domain
369 was set equal to 20 cm. The grid was set uniform with a grid spacing of $\Delta z = 0.1$ cm, and the
370 time step was allowed to vary without exceeding a maximum time step of 144 s as in Chen et
371 al. [2000b] and Chen and Rolston [2000].

372

373 **3.1.2. Numerical simulation of water transport under severe dryness conditions**

374

375 The water transport model described above and the present soil-water function were
376 used to simulate the LW2, a low initial water content experiment performed by Chen et al.
377 [2000b]. In this experiment, a soil column of about 20 cm length was subject to a continuous
378 evaporation condition at surface. The relative humidity of the sweep gas alternately changed
379 from wet to dry conditions (dry N_2 , with relative humidity 0%; wet air, with relative humidity
380 97%). The evaporation experiment consisted of five periods: a first wet air period, from 0 to

381 147.1 h; a first dry N₂ period, from 147.1 to 268.6 h; a second wet air period, from 268.6 to
382 387.1 h; a second dry N₂ period, from 387.1 to 501.4 h and a third and last wet air period,
383 from 501.4 to 625.7 h. The soil was Yolo silt loam, for which the water adsorption BET
384 parameters are [Chen *et al.*, 2000a]: $B = 128.07$ and $W_m = 15$ (mg/g). Because the lack of
385 explicit experimental data in the work of Chen *et al.* [2000b], we used their fitted retention
386 curve and the experimental adsorption data given by Chen *et al.* [2000a] to fit our retention
387 function, with an estimated porosity of $\varepsilon = 0.52$. The fitting parameters and the assessment of
388 its accuracy are shown in Tables 2 and 3, respectively. Figure 3 shows the present retention
389 curve fitted by the procedure described in section 2, together with the experimental water
390 adsorption data and the Campbell retention curve obtained by Chen *et al.* [2000b] for
391 saturations below 0.2. Above $S = 0.2$ (not shown) and with $\theta_r = 0$ both Campbell and BC are
392 the same expressions and, as a result of the fit, they almost coincide for this Yolo silt loam.
393 For $P_1 > P > P_2$ both Campbell and the present model fit the experimental data well. However,
394 for $P < P_2$ only the proposed SWR follows the experimental data trend and values.

395 The molecular diffusion coefficient for water vapor in air and N₂ at 25 °C, and the
396 mass-transfer coefficient of water vapor at the soil surface were taken from Chen *et al.*
397 [2000b]. The relative permeability was calculated according to Campbell's model [Campbell,
398 1974] with the parameters given by Chen *et al.* [2000b].

399 Figure 4a shows the measured evolution of the water remaining in the soil and the
400 values calculated using Campbell and present model. The weight variation is fairly well
401 predicted by the water transport model using any of the retention curves, with a maximum
402 difference of 1.3% between data and simulation results. This coincidence is not surprising
403 when one considers that the region below P_2 of the SWR is only attained close to the surface
404 and for short periods of time (see below). Figure 4b shows the measured and simulated
405 volumetric liquid content profile at the end of the experiment. Below a depth of 5 cm the

406 calculated and measured values were very similar. Between the surface and a depth of 5 cm,
407 matric pressures were high enough to show some θ_w differences between both the calculated
408 curves. In this close-to-the-surface region, it seems that the present proposal describes most of
409 the experimental profile better, although the value measured at the surface shows a change in
410 tendency that is not predicted by the Campbell curve or the present proposal. The origin of
411 this discrepancy is not known, but it should be taken into account that it is more difficult to
412 measure water content near the soil surface, where steep gradients of the different variables in
413 this zone develop more easily.

414 For the same experiment, the dynamics of the volumetric water content at two depths
415 is shown in Figure 5. The calculated volumetric water contents followed the general trend of
416 measured water content using any of the two SWR models, but did not perfectly matched the
417 experimental data, particularly in the near-surface soil region. Note that TDR measurements
418 give an average value of volumetric water content between the rods. For the measurements at
419 the nominal depth of 1 cm, the two-probe TDR rods were 1 cm apart. Then, assuming a rod
420 diameter of 3 mm ($\sim 1/8$ "), the water content measured at 1 cm depth will be an average value
421 between 0.35 and 1.65 cm. In Figure 5, the solid lines that represent the calculated water
422 content evolution at 0.35 and 1.65 cm should encompass the reported experimental values at
423 1cm of nominal depth. It can be seen that the experimental data is within this band during the
424 wet air periods, but most of the values lie outside it during the dry N_2 periods. At the depth of
425 10 cm, the volumetric water content was measured by a TDR with rods that were 2 cm apart.
426 Figure 5 shows that these two calculated lines and the experimental data practically coincide
427 during the first wet air and dry N_2 periods. After the first dry N_2 period, the calculated lines
428 start to deviate one from the other, reaching a maximum difference of 8.3% at the end of the
429 simulation. Despite this difference, the experimental data are encompassed by the two
430 calculated lines representing the nominal depth of the TDR probe. This illustrative figure

431 shows how the mechanism that dominates the water retention at any time and some depths
432 varies during the simulation. For this Yolo silt loam, a water content of $0.027 \text{ (m}^3/\text{m}^3)$
433 corresponds to the matching point below which BET adsorption dominates, while between
434 this water content and $\theta_{w1} = 0.114 \text{ m}^3/\text{m}^3$ ($P_1 = -1.5 \text{ MPa}$) the generalized Bradley's isotherm
435 governs water retention. Above θ_{w1} there is the capillary region.

436 Figure 5 shows that during the dry N_2 periods, the simulated water content near the
437 soil surface enters the BET adsorption region, which indicates that this nearly dry region is
438 attainable under natural evaporation conditions. In addition, in the experiments of *Chen et al.*
439 [2000b] they measured the relative humidity at surface and at various depths, and their
440 measurements show that relative humidities at the surface were well below 30% during the
441 dry N_2 periods. This indicates that at least at the surface the water content is governed by
442 adsorption mechanisms that are well described by the proposed water retention curve.

443 It is worth noting that *Gee et al.* [1992] measured matric pressures in three soil
444 samples of different textures taken from sites near Richland, WA. They reported matric
445 pressures ranging from -204 to -264 MPa on the surface (0 to 1 cm). All these values are well
446 within the BET region of the proposed SWR model ($P_2 < -162 \text{ MPa}$), which suggests that
447 there is a need for SWR models that provide a detailed description of the region of very low
448 matric pressures, at least in arid regions and close to the surface.

449

450 **3.2. Water and Chemical transport simulation**

451

452 It is well known [*Chiou and Shoup*, 1985; *Chen et al.*, 2000a, 2000b; *Chen and*
453 *Rolston*, 2000] that chemical sorption on soils is greatly influenced by relative humidity.
454 Therefore, a physically accurate description of how moisture behaves in a very dry soil is also
455 expected to improve chemical transport and volatilization simulations. Transport models of

456 highly sorbing solutes in the vadose zone assume that the solid-gas and solid-liquid
457 equilibrium relationships for chemicals are influenced by the fraction of the solid surface area
458 not covered by water molecules.

459

460 **3.2.1. Governing equations and numerical implementation**

461 The chemical equilibrium relationships between the solid and fluid phases were
462 calculated according to the proposal by *Chen et al.* [2000a], who considered that organic
463 chemicals in soils are adsorbed onto water-solid and air-solid interfaces and dissolved in the
464 soil solution. In this approach, the chemical concentration at the solid-fluid interfaces is
465 affected by the fraction of the surface area not covered by water molecules, η , which depends
466 on the relative humidity of the air-soil phase, x . The fraction η can be calculated by
467 considering that the water vapor sorption follows the BET model [*Hill, 1946; Chen et al.,*
468 2000a]

469

$$470 \quad \eta(x) = \frac{1-x}{1-x+Bx} \quad (13)$$

471

472 The chemical transport equation is given by [*Silva and Grifoll, 2007*]

473

$$474 \quad \frac{\partial C_{sm}}{\partial t} = -\frac{\partial}{\partial z} (J_l + J_g + q_l C_l) \quad (14)$$

475

476 where C_{sm} (kg/m^3) is the chemical concentration in the soil matrix, C_l (kg/m^3) is the chemical
477 concentration in the liquid-phase and J_i ($\text{kg/m}^2\text{-s}$) ($i = g, l$) is the diffusive-dispersive mass
478 flux of chemical.

479 Like for water transport (Eq. 12), a dynamic boundary condition at the surface was set
480 to accommodate the volatilization flux, which was calculated by considering a mass transfer
481 limitation from the soil surface to the bulk atmosphere [Brutsaert, 1975; Grifoll and Cohen,
482 1994]. The boundary condition at the bottom was set as zero ethanol diffusive flux.

483 The governing equation for chemical transport (Eq.14) was solved with water content
484 and liquid-phase velocities evaluated from equations (9) and (10), using a fully implicit
485 scheme. The resulting discretized equations were a linear algebraic system with a tridiagonal-
486 coefficient matrix, which was solved by the Thomas algorithm [Patankar, 1980; Press et al.,
487 1986-1992].

488

489 **3.2.2. Numerical simulation of water and chemical transport under severe dryness** 490 **conditions**

491 The performance of the present model has also been evaluated in a hypothetical
492 numerical experiment of water and chemical transport and compared with the results obtained
493 by using the MS-N retention function. In this experiment, a 1-meter-long Royal soil column
494 (with retention data shown in Figures 1e and 2a) with a uniform water content of $0.25 \text{ m}^3/\text{m}^3$
495 was subject to an initial period of continuous evaporation for 4800 h, leading to very dry
496 conditions, especially near the soil surface. After this initial period of 4800 h, the second stage
497 of the experiment consisted of the simultaneous evaporation of water and the volatilization of
498 an ethanol-contaminated layer situated at a depth of between 0.1 and 0.2 m, with an initial
499 concentration in the soil-matrix equal to $1.0 \text{ kg}/\text{m}^3$, for 1200 h. The relative humidity of the
500 atmosphere was set to 15% in both stages. This condition is well representative of some
501 regions with hyper-arid climates [e.g. McKay et al., 2003].

502 The ethanol partition coefficient at the air-solid interface was calculated according to
503 Goss [1994], whereas the ethanol partition coefficient at the water-solid interface was

504 estimated as suggested by *Grifoll and Cohen* [1996]. The molecular diffusion coefficients for
505 water and ethanol vapor in air, and the molecular diffusion coefficient for ethanol in water at
506 20 °C were taken from *Reid et al.* [1987]. The dispersion coefficient was calculated following
507 the model of *Grifoll et al.* [2001] with a dispersivity at saturation set to 0.5 cm. The
508 atmosphere-side mass-transfer coefficients of water and ethanol vapors at the soil surface
509 were estimated according to *Brutsaert* [1975]. The relative permeability was calculated using
510 Campbell's model [*Campbell*, 1974] with the parameters given by *Morel-Seytoux and Nimmo*
511 [1999]. The Campbell conductivity model was chosen for two reasons. Firstly, in the dry
512 range the hypotheses underlying such models as Burdine and Mualem do not hold. Secondly,
513 *Morel-Seytoux and Nimmo* [1999] also used the Campbell expression to calculate the
514 hydraulic conductivity. So, this conductivity model enables comparisons to be made that only
515 depend on the SWR functions.

516 The evolution of water evaporation and ethanol volatilization fluxes determined by the
517 MS-N retention function and the present model are compared in Figure 6. As shown in Figure
518 6a, both retention functions show the classical first stage of water evaporation at constant-rate.
519 The falling-rate stage started at about $t = 350$ h with the MS-N retention function and at about
520 $t = 600$ h with the present model. Because of this delay at the beginning of the falling-rate
521 stage, there was a period in which the evaporation flux obtained with MS-N was lower than
522 the flux obtained with the present retention function. However, from about $t = 1250$ h the
523 tendency was for the evaporation flux obtained with the present model to be lower than the
524 flux obtained with the MS-N function. This was because, as the top soil dries, lower water
525 contents were obtained with the MS-N retention model in that region. This result is consistent
526 with the SWR fits because, for a given matric suction and within the transition and BET
527 ranges, the water content predicted by the present approach is higher than the water content
528 predicted by the MS-N function (see Figs. 1e and 2a). As a consequence, the lower water

529 contents increased the water vapor diffusion within the top soil, which significantly increased
530 the evaporation flux in the simulation with the MS-N retention function. The evolution of
531 water content at various depths is shown in Figure 7. In general, within the first 10 cm
532 adjacent to the soil surface, the water content was lower with the MS-N function, although
533 there were some periods during which this was not the case. By contrast, the present approach
534 led to lower water contents at depths greater than 50 cm. The comparison between the soil
535 surface and 5 cm-depth curves, and between a depth of 10 cm and 50 cm-depth curves shows
536 that water content gradients were higher during the MS-N simulation. These higher gradients
537 were responsible for increased water vapor diffusion and a greater evaporation rate (Figure
538 6a). Note that when the MS-N function was used, at the end of the first stage ($t = 350$ h) the
539 water content was lower than $0.02 \text{ m}^3/\text{m}^3$: i.e. $S < 0.06$, a range in which the present approach
540 fits the experimental data better than the MS-N model (see Figure 2a). Also, at $t = 4800$ h the
541 whole soil reached the BET conditions with the present retention model. On the other hand, at
542 depths greater than 0.5 m, the MS-N retention function led to water contents higher than
543 $0.017 \text{ m}^3/\text{m}^3$, the upper limit of the BET adsorption range.

544 The use of one retention function or another also led to differences in the transport
545 behavior of ethanol. The concentration of ethanol within the soil was lower and the ethanol
546 volatilization fluxes were higher with the MS-N retention function (see figure 6b). This was
547 because the lower relative humidity that developed in the top soil during the simulation with
548 the present model increased the availability of adsorption sites, which led to a lower
549 volatilization flux than when the MS-N model was used. Additionally, the lower water
550 contents resulting from the MS-N simulation increased the transport of ethanol by gas-phase
551 diffusion within the top soil, which also favored the volatilization flux. Note that in both, the
552 simulations with the MS-N and the present model, the chemical equilibrium between the solid
553 and fluid phases has been calculated with a BET adsorption isotherm (in fact, the BET part of

554 the present model), as is indicated in Eq. 13. However, Figures 2a and 6b show that the use of
555 an extended retention function that differs from the adsorption experimental data could lead to
556 significant differences of the calculated chemical volatilization fluxes.

557

558 **4. Conclusions**

559 A new full-range SWR function with physical consistence in the dry range has been
560 proposed. The approach takes advantage of the physical consistency and robustness of the
561 BET adsorption isotherm to describe the very dry end, while preserving the capillary behavior
562 of the classical BC function in the wet range. The transition from capillary to adsorption
563 mechanisms is accomplished by a generalization of the Bradley's isotherm, through a
564 relationship between the logarithmic of the matric suction and a cubic polynomial of the water
565 content. Continuity of the function and its derivative is assured through the different regions.

566 The validity range of the BET adsorption isotherm was established for a relative
567 humidity below 30%. The generalized Bradley's isotherm was used between this point and
568 $P_1 = -1.5$ MPa, above which the classical BC function was chosen because classical models of
569 water retention work well in the wet range of soil water.

570 The proposed water-retention curve is quite similar to other full-range SWR models in
571 most of the saturation range. However, the limiting behavior of matric pressure as dryness is
572 approached is different: while most extended functions predict a finite matric pressure at zero
573 water content, the present proposal predicts an infinite matric pressure according the
574 adsorption theories. Therefore, in simulations using one or the other approaches one could
575 expect differences in situations of low water content. Also, these differences affect the
576 calculations of organic chemicals transport, since adsorption is highly dependent on relative
577 humidity.

578

579 **Acknowledgments**

580

581 We gratefully acknowledge the financial assistance received from the DGICYT of Spain,
582 under project FIS2005-07194 and from the Generalitat de Catalunya (2005SGR-00735). We
583 also acknowledge the support received from the DURSI and the European Social Fund.

584 **References**

- 585 Agam, N. and P. R. Berliner (2006), Dew formation and water vapor adsorption in semi-arid
586 environments. A review. *J. Arid Environ.* 65, 572–590.
- 587 Amali, S., L. W. Petersen, and D. E. Rolston (1994), Modeling multicomponent volatile
588 organic and water vapor adsorption on soils *J. Hazardous Mater.*, 36, 89-108.
- 589 Andraski, B. J., and E. A. Jacobson (2000), Testing a full-range soil water retention function
590 in modeling water potential and temperature, *Water Resour. Res.*, 36(10), 3081-3089.
- 591 Baggio, P., C. Bonacina, and B. A. Schrefler (1997), Some considerations on modeling heat
592 and mass transfer in porous media, *Transport Porous Med.*, 28, 233-251.
- 593 Batterman, S., A. Kulshrestha and H. Y. Cheng (1995), Hydrocarbon vapor transport in low
594 moisture soils. *Environ. Sci. Technol.*, 29, 171-180.
- 595 Bear, J., and Y. Bachmat (1991), *Introduction to modeling of transport phenomena in porous*
596 *media*. Kluwer academic publishers, Dordrecht.
- 597 Bradley, R. S. (1936), Polymolecular adsorbed films, *J. Chem. Soc.*, 139, 1467-1474.
- 598 Brooks, R. H., and A. T. C. Corey (1964), Hydraulic properties of porous media, in *Hydrol.*
599 *Pap. 3*, Colo. State Univ., Fort Collins.
- 600 Brutsaert, W. (1975), A theory for local evaporation (or heat transfer) from rough and smooth
601 surfaces at ground level, *Water Resour. Res.*, 11(4), 543-550.
- 602 Burdine, N. T. (1953), Relative permeability calculations from pore-size distribution data,
603 *Petroleum Trans.*, 198, 71-77.
- 604 Burns, E. R., J.-Y. Parlange, J. S. Selker, and R. B. Guenther (2006a), Thermodynamic
605 correction for salts in variably saturated porous media, *Transport Porous Med.*, 63, 381-
606 398.

607 Burns, E. R., J.-Y. Parlange, J. S. Selker, and R. B. Guenther (2006b), Effects of sodium
608 chloride on constitutive relations in variable saturated porous media, *Water Resour. Res.*,
609 42, W05405, doi:10.1029/2005WRRR004060.

610 Campbell, G. S. (1974), A simple method for determining unsaturated conductivity from
611 moisture retention data, *Soil Sci.*, 117, 311-314.

612 Campbell, G. S., and S. Shiozawa (1992), Prediction of hydraulic properties of soils using
613 particle size distributions and bulk density data, in *International Workshop on Indirect
614 Methods for Estimating the Hydraulic Properties of Unsaturated Soils*, Univ. of Calif.
615 Press, Berkeley.

616 Campbell, G. S., J. D. Jungbauer Jr., S. Shiozawa, and R. D. Hungerford (1993), A one-
617 parameter equation for water sorption isotherms of soils, *Soil Science*, 156(5), 302-305.

618 Cassel, D. K., and D. R. Nielsen (1986), Field capacity and available water capacity, in
619 *Methods of Soil Analysis, Part 1. Physical and Mineralogical Methods*. Agron. Monogr. 9,
620 901-926, 2nd ed. ASA and SSSA, Madison.

621 Chen D., D. E. Rolston, and T. Yamaguchi (2000a), Calculating partition coefficients of
622 organic vapors in unsaturated soil and clays, *Soil Sci.*, 165(3), 217-225.

623 Chen D., D. E. Rolston, and P. Moldrup (2000b), Coupling diazinon volatilization and water
624 evaporation in unsaturated soils: I. Water transport, *Soil Sci.*, 165(9), 681-689.

625 Chen D., and D. E. Rolston (2000), Coupling diazinon volatilization and water evaporation in
626 unsaturated soils: II. Diazinon transport, *Soil Sci.*, 165(9), 690-698.

627 Chiou, C. T., and T. D. Shoup (1985), Soil sorption of organic vapors and effects of humidity
628 on sorptive mechanism and capacity, *Environ. Sci. Technol.*, 19, 1196-1200.

629 de Seze, G., K. T. Valsaraj, D. D. Reible, and L. J. Thibodeaux (2000), Sediment-air
630 equilibrium partitioning of semi-volatile hydrophobic organic compounds. Part 1. Method
631 development and water vapor sorption isotherm, *Sci. Total Environ.*, 253, 15-26.

632 Fayer, M. J., and T. L. Jones (1990), UNSAT-H Version 2.0: Unsaturated soil water and heat
633 flow model, *Publ. PNL-6779*, Pac. Northwest Lab., Richland, Wash.

634 Fayer, M. J., and C. S. Simmons (1995), Modified soil water retention functions for all matric
635 suctions, *Water Resour. Res.*, *31*, 1233-1238.

636 Fink, D. H., and R. D. Jackson (1973), An equation for describing water vapor adsorption
637 isotherms of soils, *Soil Sci.*, *116*, 256-261.

638 Gawin, D., F. Pesavento, and B. A. Schrefler (2002), Modelling of hygro-thermal behaviour
639 and damage of concrete at temperature above the critical point of water, *Int. J. Numer.*
640 *Anal. Meth. Geomech.*, *26*, 537-562.

641 Gee, G. W., M. D. Campbell, G. S. Campbell and J. H. Campbell (1992), Rapid measurement
642 of low soil water potentials using a water activity meter, *Soil Sci. Soc. Am. J.*, *56*, 1068-
643 1070.

644 Goss, K.-U. (1994), Adsorption of organic vapors on polar mineral surfaces and on a bulk
645 water surface: development of an empirical predictive model, *Environ. Sci. Technol.*, *28*,
646 640-645.

647 Goss, K.-U., and M. Madliger (2007), Estimation of water transport based on in situ
648 measurements of relative and temperature in a dry Tanzanian soil, *Water Resour. Res.*, *43*,
649 W05433, doi: 10.1029/2006WR005197.

650 Grant, S. A., and R. S. Sletten (2002), Calculating capillary pressures in frozen and ice-free
651 soils below the melting temperature, *Environ. Geol.*, *42*, 130-136.

652 Grifoll, J., and Y. Cohen (1994), Chemical volatilization from the soil matrix: Transport
653 through the air and water phases, *J. Hazard. Mater.*, *37*, 445-457.

654 Grifoll, J., and Y. Cohen (1996), Contaminant migration in the unsaturated soil zone: the
655 effect of rainfall and evapotranspiration, *J. Contam. Hydrol.*, *23*, 185-211.

656 Grifoll, J., J. M. Gastó, and Y. Cohen (2005), Non-isothermal soil water transport and
657 evaporation, *Adv. Water Resour.*, 28(11), 1254-66.

658 Groenevelt, P. H., and C. D. Grant (2004), A new model for the soil-water retention curve that
659 solves the problem of residual water contents, *Eur. J. Soil Sci.*, 55, 479-485.

660 Hill, T. (1946), Theory of multimolecular adsorption from a mixture of gases, *J. Chem. Phys.*,
661 14(4), 268-275.

662 Jin, Y., and A. Jury (1996), Characterizing the dependence of gas diffusion coefficient on soil
663 properties, *Soil Sci. Soc. Am. J.*, 60, 66-71.

664 Kelley, C. T. (1995), *Iterative methods for linear and nonlinear equations*, SIAM,
665 Philadelphia.

666 Lasdon, L. S., A. D. Warren, A. Jain, and M. Ratner (1978), Design and testing of a
667 generalized reduced gradient code for nonlinear programming, *ACM Trans. Math.*
668 *Software*, 1, 34-50.

669 McKay, C. P., E. I. Friedmann, B. Gómez-Silva, L. Cáceres-Villanueva, D. T. Andersen, and
670 R. Landheim (2003), Temperature and moisture conditions for life in the extreme arid
671 region of the Atacama Desert: four years of observations including the El Niño of 1997-
672 1998. *Astrobiology*, 3(2), 393-406.

673 Morel-Seytoux, H. J., and J. R. Nimmo (1999), Soil water retention and maximum capillary
674 drive from saturation to oven dryness, *Water Resour. Res.*, 35(7), 2031-2041.

675 Mualem, Y. (1976), A new model for predicting the hydraulic conductivity of unsaturated
676 porous media, *Water Resour. Res.*, 12, 513-522.

677 Nimmo, J. R. (1991), Comment on the treatment of residual water content in “A consistent set
678 of parametric models for the two-phase flow of miscible fluid in the Subsurface” by L.
679 Luckner et al., *Water Resour. Res.*, 27, 661-662.

680 Or, D., and M. Tuller (1999), Liquid retention and interfacial area in variably saturated porous
681 media: Upscaling from single-pore to sample-scale model, *Water Resour. Res.*, 35(12),
682 3591-3605.

683 Orchiston, H. D. (1952), Adsorption of water vapor: I. Soils at 25 °C, *Soil Sci.*, 76, 453-465.

684 Patankar, S. V. (1980), *Numerical heat transfer and fluid flow*, McGraw-Hill, New York.

685 Pennell, K. D., R. D. Rhue, P. S. C. Rao, and C. T. Johnston (1992), Vapor-phase sorption of
686 *p*-xylene and water on soils and clay minerals, *Environ. Sci. Technol.*, 26, 756-763.

687 Press, W. H., S. A. Teukolsky, W. T. Vetterling, and B. P. Flannery (1986-1992), *Numerical*
688 *recipes in fortran 77: the art of scientific computing*, Cambridge University Press, New
689 York.

690 Puri, A. N., E. M. Crowther, and B. A. Keen (1925), The relation between the vapour pressure
691 and water content of soils, *J. Agric. Sci.*, 15, 68-88.

692 Rawls, W. J., and D. L. Brakensiek (1989), Estimation of soil water retention and hydraulic
693 properties, in *Unsaturated flow in hydrology modeling, theory and practice*, Kluwer
694 Academic Publishers.

695 Reid, R. C., J. M. Prausnitz, and B. E. Poling (1987), *The properties of gases and liquids*,
696 McGraw-Hill Inc., New York.

697 Rhue, R. D., K. D. Pennell, P. S. C. Rao, and W. H. Reve (1989), Competitive adsorption of
698 alkylbenzene and water vapors on predominantly mineral surfaces, *Chemosphere*, 18(9-
699 10), 1971-1986.

700 Ross, P. J., J. Williams, and K. L. Bristow (1991), Equation for extending water-retention
701 curves to dryness, *Soil Sci. Soc. Am. J.*, 55, 923-927.

702 Rossi, C., and J. R. Nimmo (1994), Modeling of soil water retention from saturation to oven
703 dryness, *Water Resour. Res.*, 30, 701-708.

704 Ruiz, J., R. Bilbao, and M. B. Murillo (1998), Adsorption of different VOC onto soil minerals
705 from gas phase: influence of mineral, type of VOC, and air humidity, *Environ. Sci.*
706 *Technol.*, *32*, 1079-1084.

707 Scanlon B. R., K. Keese, R. C. Reedy, J. Simunek, and B. J. Andraski (2003), Variations in
708 flow and transport in thick desert vadose zones in response to paleoclimatic forcing (0–90
709 kyr): field measurements, modeling, and uncertainties, *Water Resour. Res.*; *39*(7), 1179.

710 Schofield, R. K. (1935), The pF of the water in soil, *Trans. Int. Congr. Soil Sci.* 3rd, II 38-48.

711 Schrefler, B. A. (2004), Multiphase flow in deforming porous material, *Int. J. Numer. Anal.*
712 *Meth. Geomech.*, *60*, 27-50.

713 Silva, O., and J. Grifoll (2007), Non-passive transport of volatile organic compounds in the
714 unsaturated zone, *Adv. Water. Resour.*, *30*(3), 794-807.

715 Tuller, M., D. Or, and L. M. Dudley (1999), Adsorption and capillary condensation in porous
716 media: Liquid retention and interfacial configurations in angular pores, *Water Resour.*
717 *Res.*, *35*(7), 1949-1964.

718 Valsaraj, K. T., and L. J. Thibodeaux (1988), Equilibrium adsorption of chemical vapors on
719 surface soils, landfills and landfarms—a review, *J. Hazardous Mater.*, *19*, 79-99.

720 Valsaraj, K. T. (1995), *Elements of environmental engineering. Thermodynamics and kinetics.*
721 Boca Raton: CRC Press Inc..

722 van Genuchten, M. T. (1980), A closed-form equation for predicting the hydraulic
723 conductivity of unsaturated flow, *Soil Sci. Soc. Am. J.*, *44*, 892-898.

724 Webb, S. W. (2000), A simple extension of two-phase characteristic curves to include the dry
725 region, *Water Resour. Res.*, *36*(6), 1425-1430.

726 Yoon, H., A. J. Valocchi, and C. W. Werth (2003), Modeling the influence of water content
727 on soil vapor extraction. *Vadose Zone J.* *2*, 368–381.

728

729 **Table captions**

730

731 **Table 1.** BET adsorption isotherm parameters from literature.

732

733 **Table 2.** Summary of soil fitting parameters.

734

735 **Table 3.** Goodness of the present SWR function fit.

736

Table 1. BET adsorption isotherm parameters from literature.

Source	Soil type	<i>B</i>	<i>W_m</i> (mg/g)
<i>Puri et al.</i> [1925]	5 different soils	15	6
<i>id.</i>	5 different soils	30	19
<i>Orchiston</i> [1952]	podzol from Otago	14.4	39.8
<i>id.</i>	red brown loam from North Auckland	15.2	33.3
<i>id.</i>	meadow soil from Great Barrier Island	13.0	37.3
<i>id.</i>	brown granular clay form North Auckland	15.2	29.8
<i>id.</i>	yellow-gray loam from Malborough	13.7	5.9
<i>id.</i>	alluvial from Canterbury	12.5	7.6
<i>id.</i>	peat soil from Canterbury	12.7	60.4
<i>Chiou and Shoup</i> [1985]	woodburn dry soil (silt soil, 21% kaolinite)	37.6	11.7
<i>Valsaraj and Thibodeaux</i> [1988]	montmorillonite (natural unheated)	21	12.56
<i>id.</i>	montmorillonite (preheated, 105 °C)	23.3	11.67
<i>id.</i>	montmorillonite (Mg-saturated, unheated)	28.4	11.67
<i>id.</i>	montmorillonite (H-saturated, unheated)	15.2	11.86
<i>id.</i>	montmorillonite (Na-saturated, unheated)	5.9	9.31
<i>id.</i>	montmorillonite (natural unheated at 35 °C)	19.6	12.07
<i>id.</i>	illite (natural unheated)	12.1	2.37
<i>id.</i>	illite (Ca-saturated, unheated)	9.2	2.67
<i>id.</i>	illite (Na-saturated, unheated)	8.5	2.83
<i>id.</i>	kaolinite (natural unheated)	37.8	0.17
<i>id.</i>	sand (green sand, unheated)	5	1.89
<i>Rhue et al.</i> [1989]	Li-kaolin	52	2.6
<i>Pennel et al.</i> [1992], <i>Rhue et al.</i> [1989]	Na-kaolin (kaolinite)	20	4.2
<i>id.</i>	silica gel	18	33.8
<i>Amali et al.</i> [1994]	Riverbed sand	25.7	2.3
<i>id.</i>	Yolo silt loam	17.6	8.5
<i>Ruiz et al.</i> [1998]	sand	7.11	0.524
<i>id.</i>	limestone	36.29	0.0412
<i>id.</i>	clay	16.13	5.28
<i>Chen et al.</i> [2000]	Yolo silt loam	128.07	15
<i>de Seze et al.</i> [2000]	natural montmorillonite	21	13
<i>id.</i>	lake sediment	53	12.4

Table 2. Summary of soil fitting parameters.

Soil	B	W_m , mg/g	P_b , Pa	λ	θ_r	$^d \epsilon$
^a Palouse	39.49	11.26	-4507	0.32	0.034	0.44
^a Palouse B	11.39	32.52	-2866	0.19	0	0.55
^a Walla Walla	23.49	9.26	-4190	0.35	0.030	0.39
^a Salkum	124.3	11.62	-9932	0.29	0	0.48
^a Royal	68.00	7.01	-3939	0.50	0.034	0.35
^a L-Soil	42.98	2.99	-1229	0.40	0.015	0.18
^b Rothamsted	1071	20.87	-15139	0.33	0	0.51
^c Yolo silt loam	128.07	15	-4630	0.27	0	0.52

^aCampbell and Shiozawa [1992]

^bSchofield [1935]

^cChen *et al.* [2000a, 2000b]

^dPorosity was fixed in accordance with measured or estimated data.

Table 3. Goodness of the present SWR function fit.

Soil	R^2 BET	RMSE	$(\Delta\theta_w)_{max}$ (v/v)	$\overline{\Delta\theta_w}$ (v/v)
^a Palouse	0.986	0.108	0.0096	0.0033
^a Palouse B	0.993	0.164	0.0134	0.0026
^a Walla Walla	0.990	0.088	0.0056	0.0015
^a Salkum	0.992	0.129	0.0077	0.0028
^a Royal	0.988	0.114	0.0028	0.0009
^a L-Soil	0.992	0.153	0.0015	0.0004
^b Rothamsted	0.999	0.129	0.0087	0.0043
^c Yolo silt loam	0.955	0.007	0.0049	0.0020

^a*Campbell and Shiozawa* [1992]

^b*Schofield* [1935]

^c*Chen et al.* [2000a, 2000b]

737 **Figure captions**

738

739 **Figure 1.** Data-model comparison for SWR functions: (a) Palouse, (b) Palouse B, (c) Walla
740 Walla, (d) Salkum, (e) Royal, (f) L-Soil, (g) Rothamsted. Dash-dotted line corresponds to
741 the MS-N model [*Morel-Seytoux and Nimmo*, 1999], while solid line is for the present
742 approach.

743

744 **Figure 2.** Comparison between experimental data, MS-N model [*Morel-Seytoux and Nimmo*,
745 1999] and the present approach represented at BET scale: (a) Royal soil, (b) L-Soil.

746

747 **Figure 3.** Present SWR model fitted to water adsorption data and Campbell model from *Chen*
748 *et al.* [2000a, 2000b] (Yolo silt loam soil).

749

750 **Figure 4.** Comparison of water transport experimental data LW2 [*Chen et al.*, 2000b] and
751 numerical simulation including the present SWR function (a) percentage of initial water
752 remaining in the soil, (b) water content profile at the end of the experiment (the dash-dotted
753 line corresponds to the initial water content).

754

755 **Figure 5.** Evolution of measured and calculated volumetric water content at different depths
756 during LW2 experiment [*Chen et al.*, 2000b]. Nominal depths for experimental data: ● 1
757 cm, ○ 10 cm. Solid lines denotes the present simulation results at the indicated depth. Dash-
758 dotted lines are for the simulation of *Chen et al.* [2000b].

759

760 **Figure 6.** Influence of water retention function on the evolution of (a) water evaporation, and
761 (b) ethanol volatilization fluxes.

762 **Figure 7.** Evolution of the volumetric water content calculated with the MS-N model [*Morel-*
763 *Seytoux and Nimmo, 1999*] and the present model.

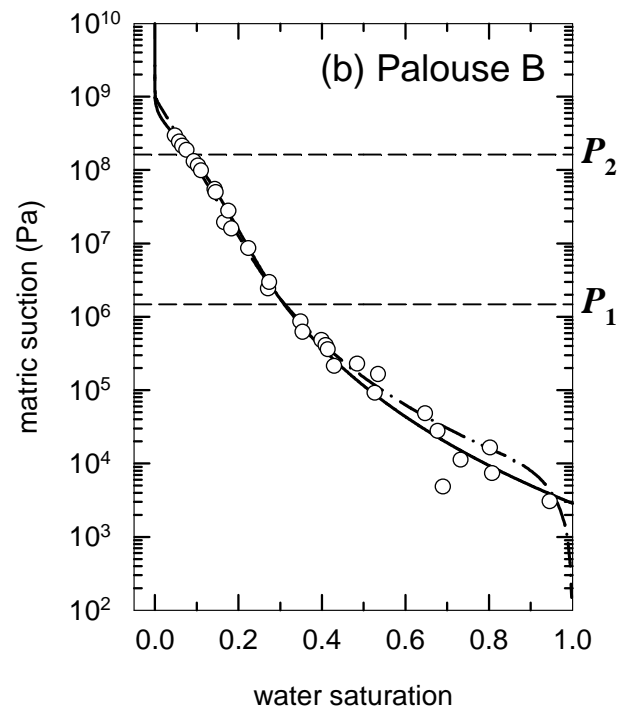
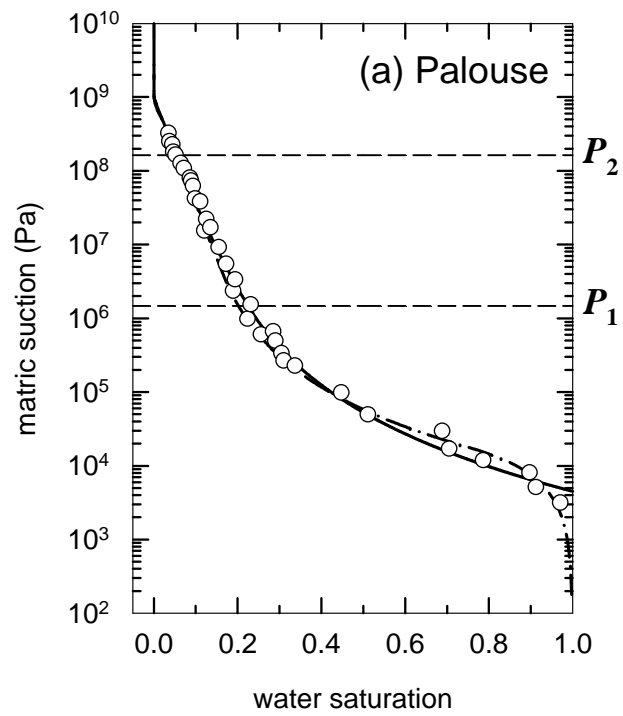


Figure 1(a)-(b)

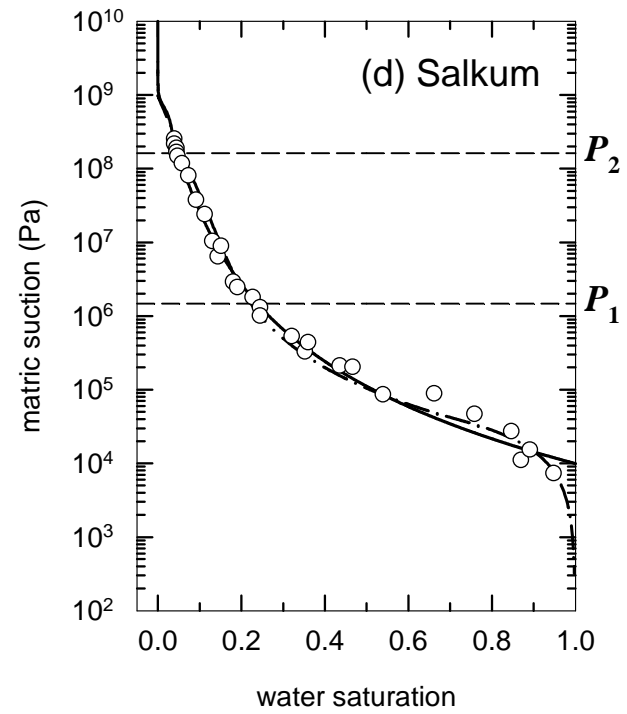
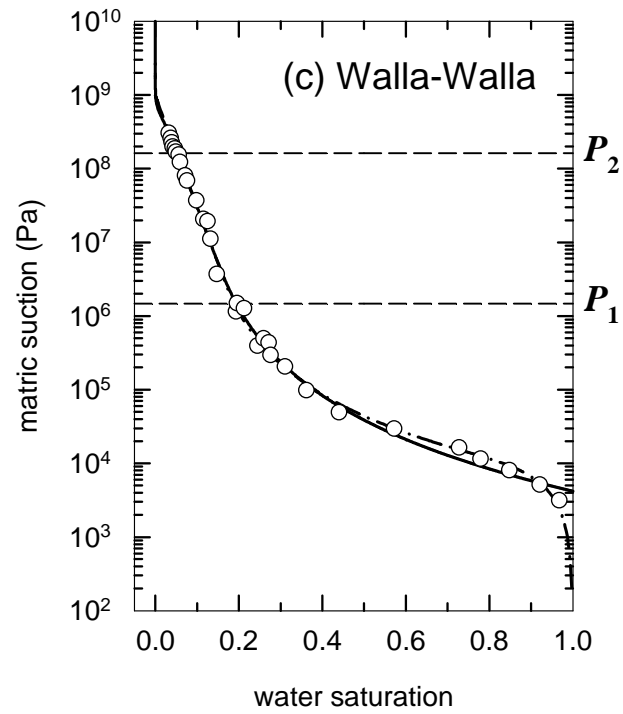


Figure 1(c)-(d)

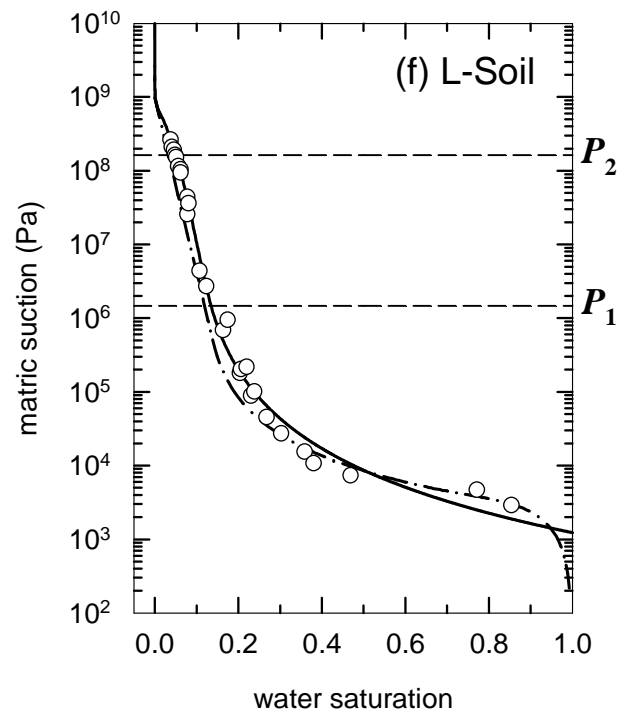
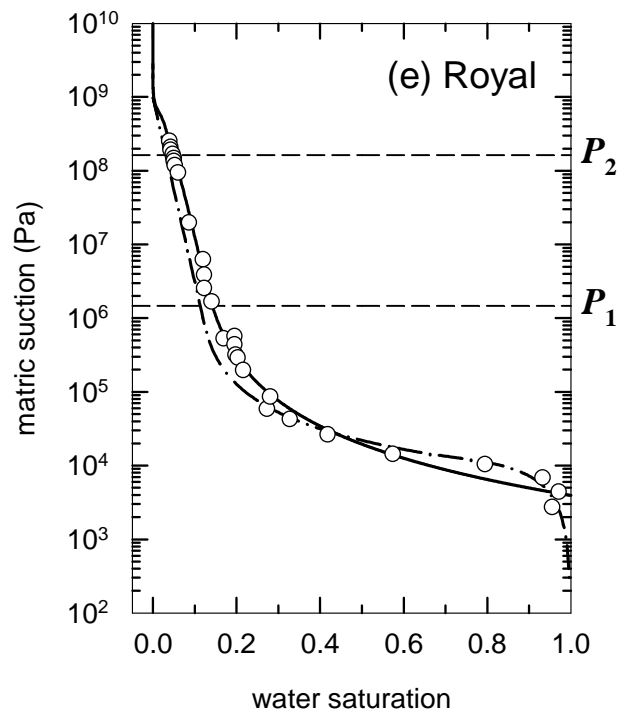


Figure 1(e)-(f)

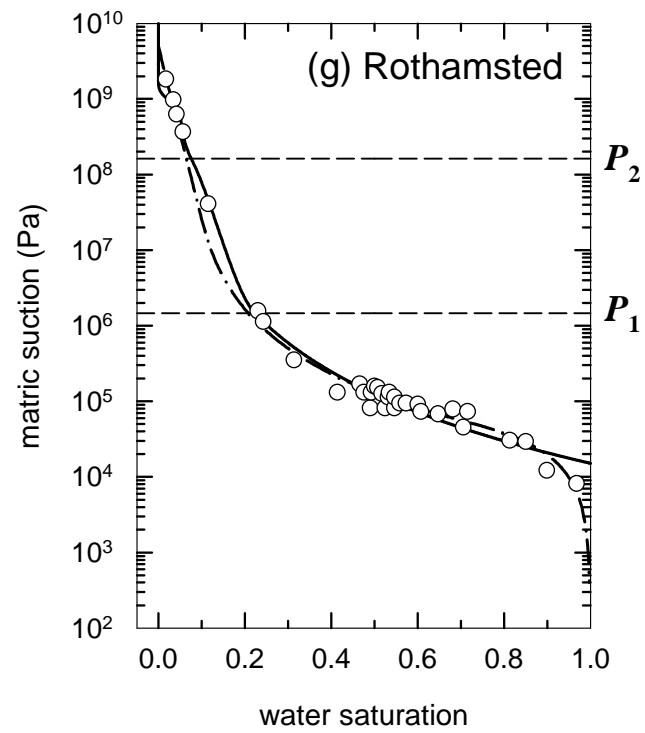


Figure 1(g)

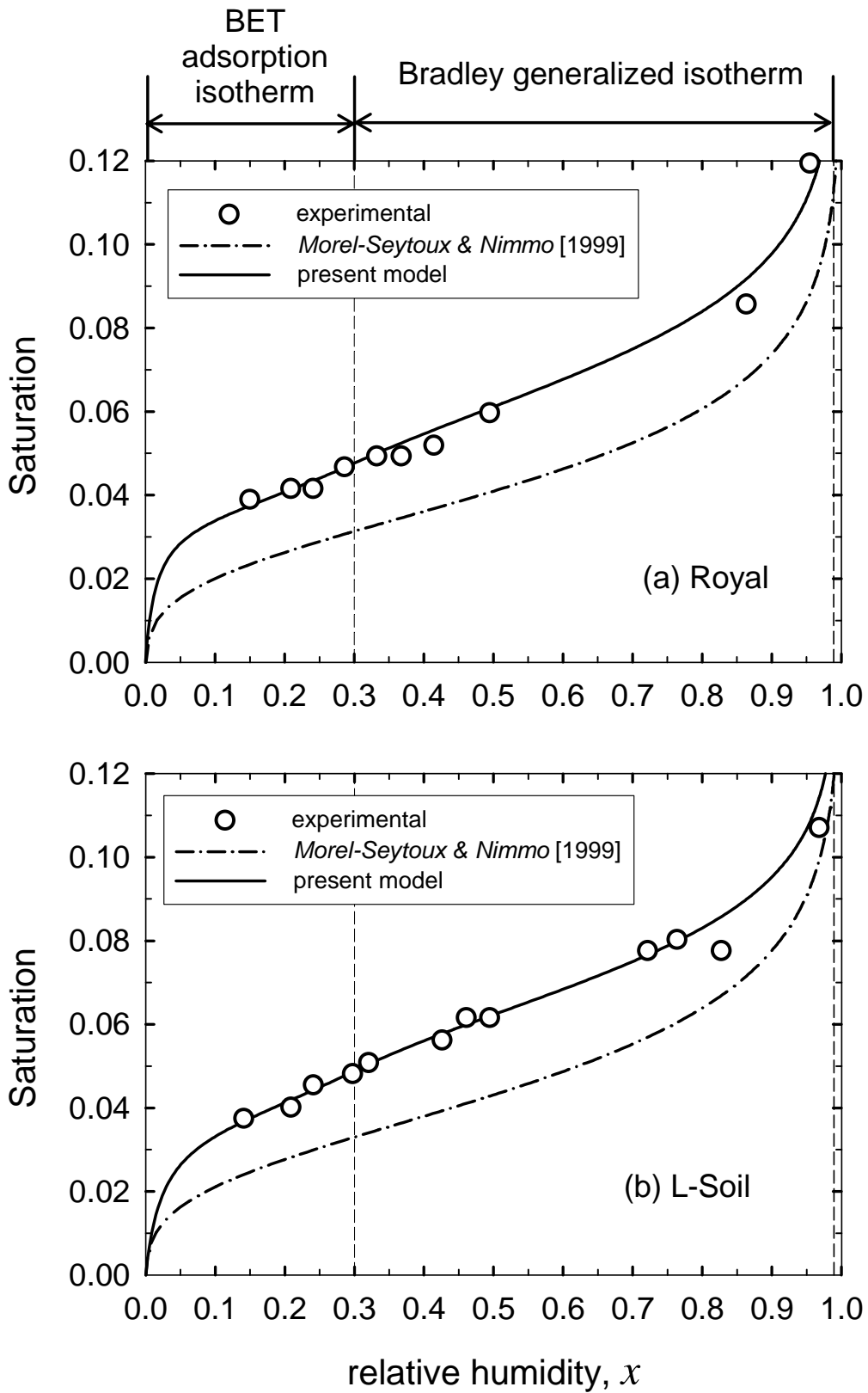


Figure 2

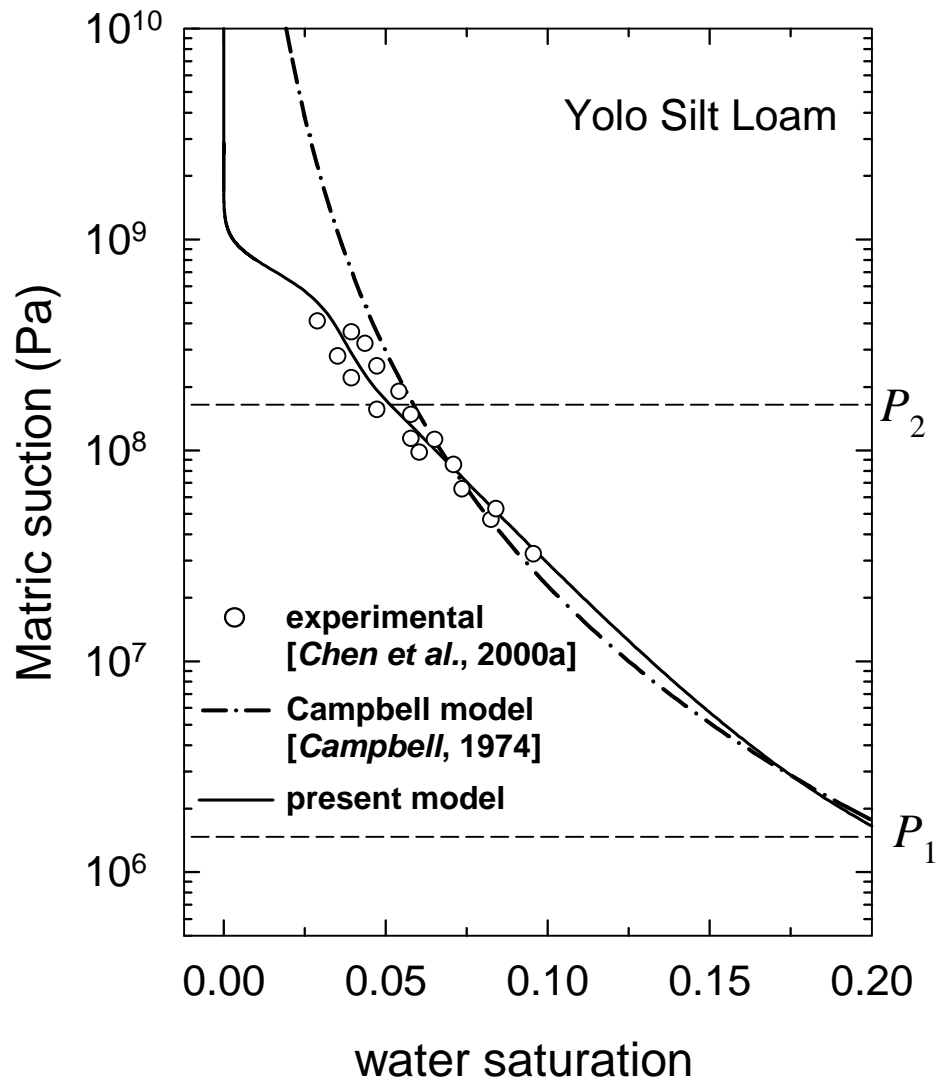


Figure 3

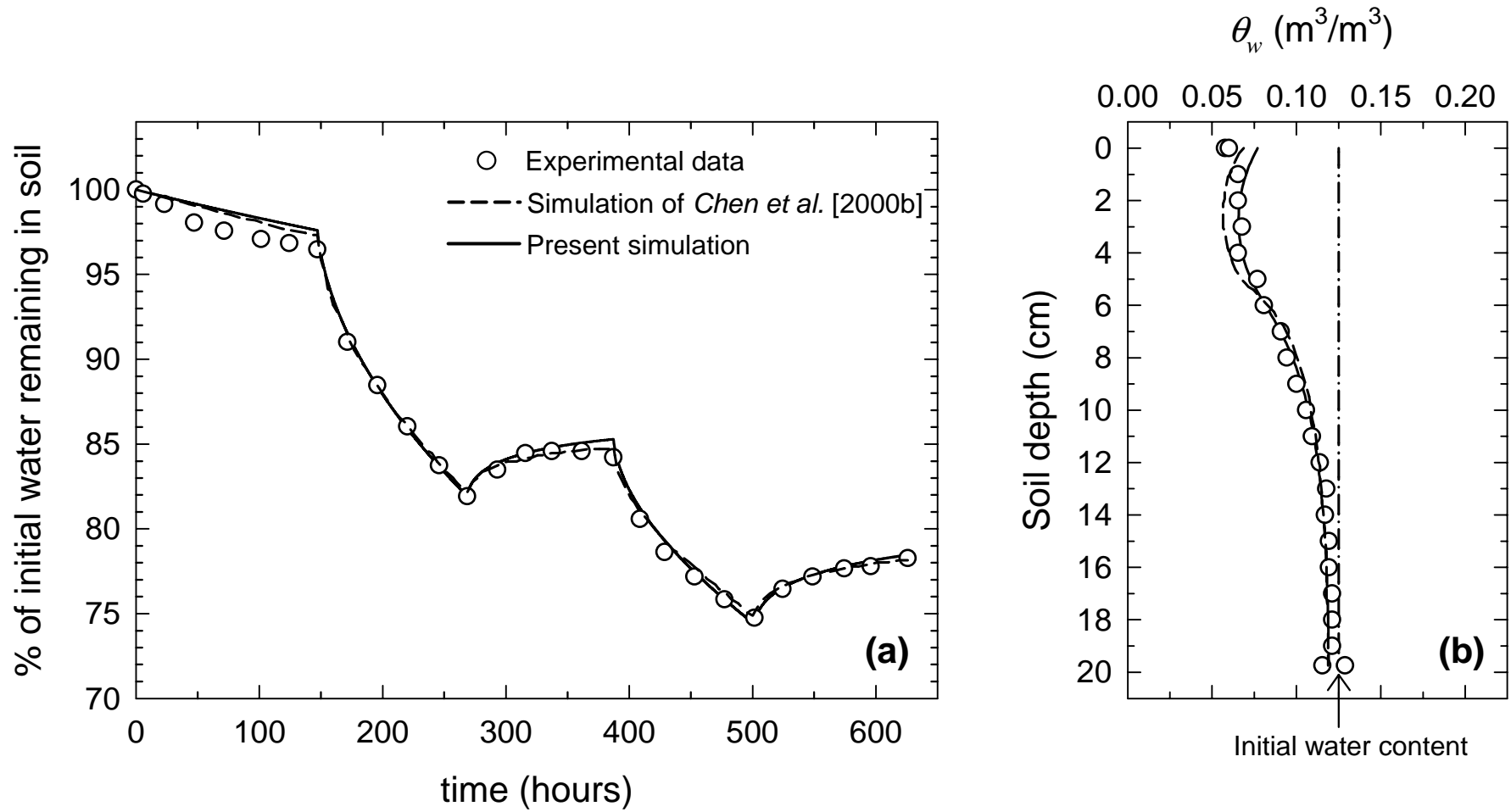


Figure 4

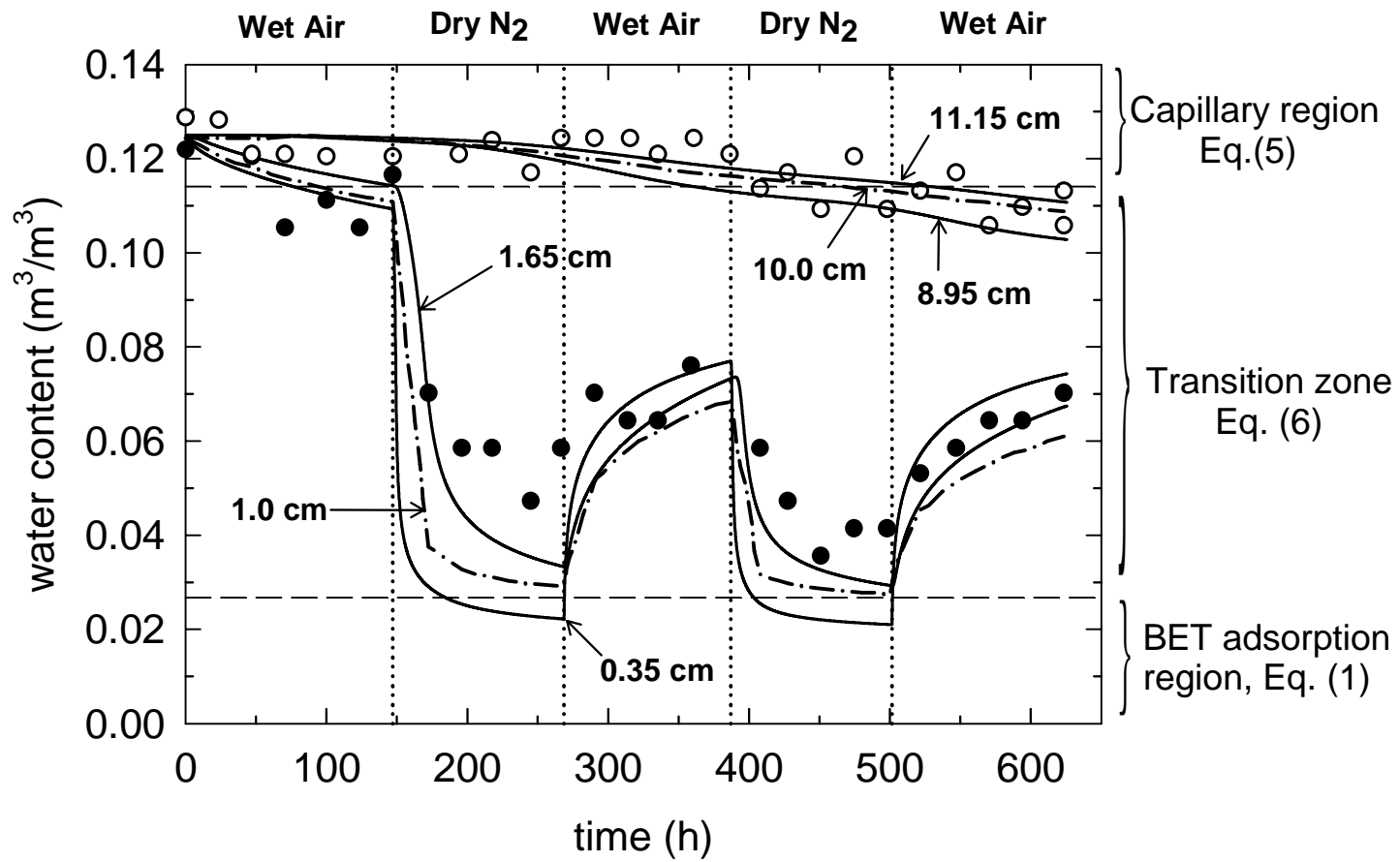


Figure 5

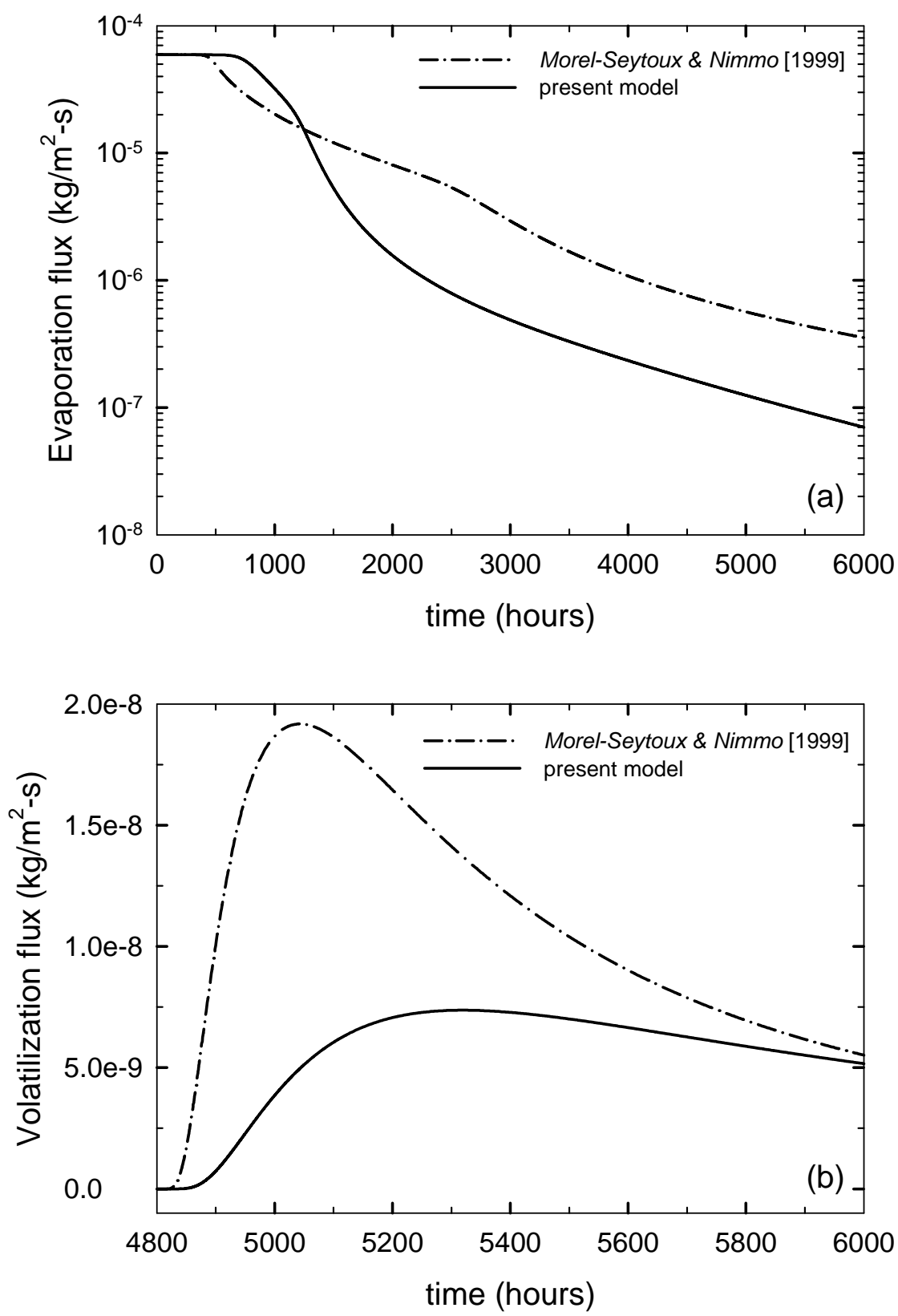


Figure 6

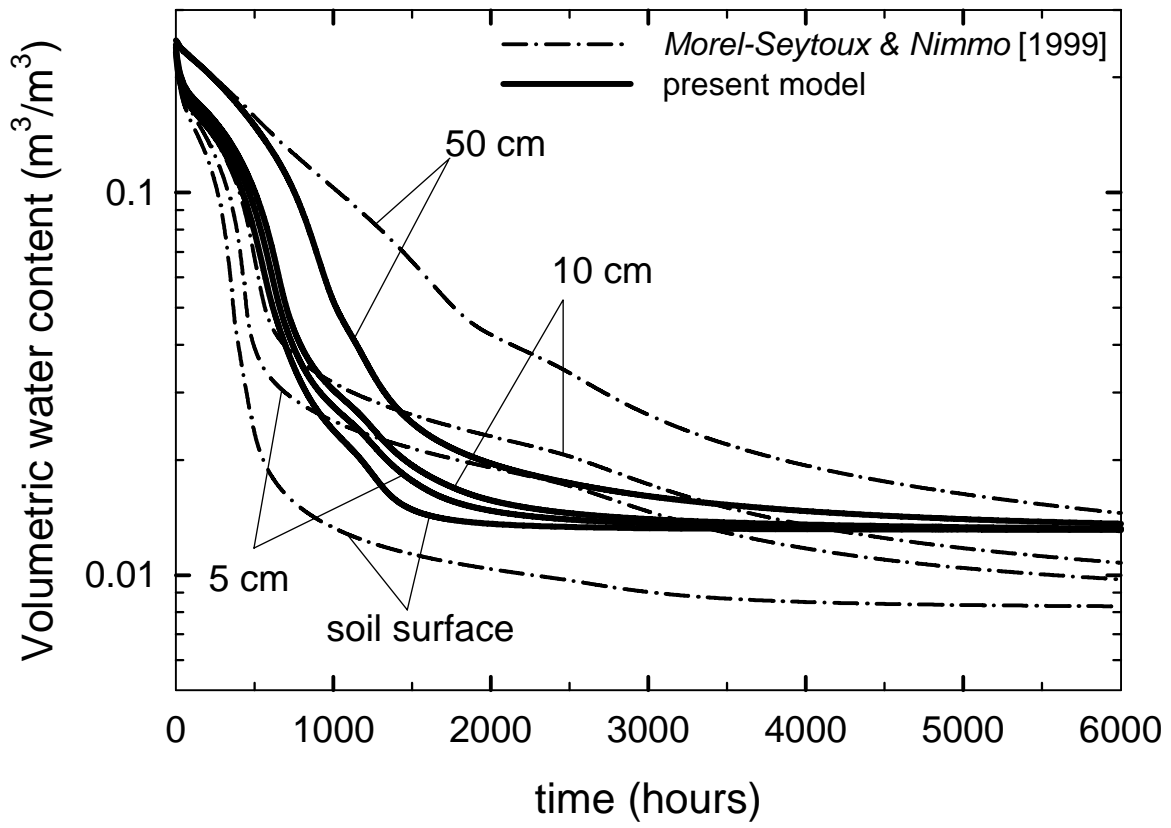


Figure 7